ELSEVIER

Materials Science and Engineering B 114–115 (2004) 312–317

MATERIALS SCIENCE & ENGINEERING B

www.elsevier.com/locate/mseb

Impact of dopant profiles on the end of range defects for low energy germanium preamorphized silicon

R.A. Camillo-Castillo[a,*], M.E. Law[b], K.S. Jones[a]

[a] SWAMP Center, Department of Materials Science and Engineering, University of Florida, Gainesville, P.O. Box 116130, Gainesville, FL 32611-6130, USA
[b] SWAMP Center, Department of Electrical and Computer Engineering, University of Florida, Gainesville, P.O. Box 116130, FL 32611-6130, USA

Abstract

As the industry continues to aggressively scale CMOS technology, the shift to lower energy ion implantation becomes essential. The consequent shallower amorphous layers result in dopant profiles that are in closer proximity to the end of range (EOR) damage and therefore a better understanding of the interaction between the dopant atoms and the EOR is required. A study is conducted on the influence of dopant profiles on the behavior of the EOR defects. Czochralski-grown silicon wafers are preamorphized with 1×10^{15} cm^{-2}, 10 keV Ge$^+$ ions and subsequently implanted with 1×10^{15} cm^{-2}, 1 keV B$^+$ ions. A sequence of rapid thermal and furnace anneals are performed at 750 °C under a nitrogen ambient for periods of 1 s up to 6 h. Plan view transmission electron microscopy (PTEM) reveals a significant difference in the defect evolution for samples with and without boron, suggesting that the boron influences the evolution of the EOR defects. The extended defects observed for samples which contain boron appear as dot-like defects which are unstable and dissolve after very short anneal times. The defect evolution however, in samples without boron follows an Oswald ripening behavior and form {3 1 1}-type defects and dislocation loops. Hall effect measurements denote a high initial activation and subsequent deactivation of the dopant atoms which is characteristic of the formation of boron interstitial clusters. Diffusion analyses via secondary ion mass spectroscopy (SIMS) support this theory.
© 2004 Elsevier B.V. All rights reserved.

Keywords: CMOS technology; Oswald ripening behavior; Hall effect

1. Introduction

Standard CMOS technology employs the formation of amorphous layers via ion implantation, prior to the introduction of the dopant atoms into the silicon lattice, for ultra shallow junction (USJ) formation. An annealing process subsequent to implantation repairs the inherent lattice damage and activates implanted dopant atoms. However, the high interstitial supersaturation in the lattice during annealing results in unwanted complex and coupled processes such as clustering, diffusion and dopant deactivation. Transient enhanced diffusion (TED) [1] is a well-researched phenomenon [2,3,4,5] that also occurs. It is due to the formation of mobile dopant complexes via the coupling of silicon interstitials with the substitutional dopant atoms. The interstitial supersaturation associated with the EOR defects, which accompany amorphization provide the interstitials necessary for TED. Solid phase epitaxial re-growth (SPER) is capable of activating dopant levels that exceed solid solubility levels in silicon, at relatively low temperatures. The low thermal budget offers good junction depth control by reducing diffusion, which is highly beneficial for USJ formation. In addition, it provides excellent compatibility with the thermal requirements of high-K dielectric materials and metal gates. As the industry attempts to achieve highly doped, shallow layers, ultra low energy (ULE) dopant ion implantation is becoming increasingly important. These ULE implants do not require deep amorphous layers, therefore lower energy preamorphizing implants can be used. Low energy amorphizing implants reduce the number of recoil atoms into the EOR. However, lowering the implant energy also reduces the proximity of the EOR to the surface resulting in high interstitial supersaturations in the vicinity of the dopant profile. These interstitial concentrations have been demonstrated to cluster with boron atoms at concentrations far below its solid solubility [6]

* Corresponding author.
E-mail address: rcami@tec.ufl.edu (R.A. Camillo-Castillo).

0921-5107/$ – see front matter © 2004 Elsevier B.V. All rights reserved.
doi:10.1016/j.mseb.2004.07.051

resulting in dopant deactivation. The proximity of the EOR to the boron profile therefore raises many concerns regarding the thermal stability of the activated junctions and the effect that the boron presence has on the EOR defect evolution.

2. Experiment

Two hundred mm, Czochralski grown, (1 0 0), n-type silicon wafers were preamorphized with 10 keV Ge^+ ions at a dose of 1×10^{15} cm^{-2} and subsequently implanted with 1 keV, 1×10^{15} cm^{-2} B^+ ions. Wafers which were not subjected to a boron implant served as the experimental control. All implants were conducted at a tilt and twist of 5° and 0°, respectively. Post-implantation processing included dicing the wafers into 1.4 cm × 1.4 cm samples and annealing at 750 °C under nitrogen ambient for times ranging 1 s through 6 h. Anneals performed for less than 5 min were conducted in an AG Associates Heat Pulse 210T rapid thermal annealer (RTA). The RTA temperature profile consisted of a 600 °C, 10 s soak and a ramp to 750 °C at a rate of 100 °C s^{-1}. Furnace anneals were utilized for anneal times of 5 min and greater and were executed in a quartz tube furnace. Plan view transmission electron microscopy (PTEM) was conducted on a Joel 200CX microscope operated at an accelerating voltage of 200 keV, to examine the extended defects in the silicon lattice. The PTEM samples were prepared by standard HF/HNO_3 backside etching methods and the extended defects imaged at g_{220} weak beam dark field (WBDF) conditions. Defect densities were ascertained by the quantification technique of Bharatan et al. [7] Dopant concentration–depth profiles were assessed by secondary ion mass spectroscopy (SIMS) using an Adept 1010 dynamic SIMS system by Physical Electronics. A 50 nA, 2 kV oxygen beam was employed at 41° to the normal to the surface with a raster of 250 mkm by 250 mkm. Sheet resistances were measured on a MMR Technologies Inc., Hall and Van der Pauw measurement system. These measurements were conducted at 90 K to reduce errors associated with leaky junctions, which result in contributions from the n-type substrate [8], thus allowing reliable sheet resistance measurements.

3. Results and discussion

B^+ implant conditions were chosen such that the boron was positioned in the vicinity of the end of range. The 10 keV Ge^+ implant formed a continuous amorphous layer of thickness 23 nm, as illustrated in Fig. 1. The boron implant produced a peak concentration of $\sim 8 \times 10^{20}$ cm^{-3} and a junction depth of 26 nm. It is evident that boron levels at the amorphous–crystalline interface were on the order of 3×10^{18} cm^{-3}, with boron extending into the EOR region. WBDF PTEM images of the extended defects observed during the annealing process, in those samples only subjected to the Ge^+ preamorphization are depicted in Fig. 2. Throughout the initial stages of annealing tiny dot-like defects were observed. However, as annealing progressed to 10 min the defects could be clearly discerned as 1 1 3-type defect configurations and a visible reduction in defect density was observed. Sustained annealing to 30 min revealed the existence of dislocation loops which were observed in the microstructure up to 4 h of annealing. The loops appeared to unambiguously evolve in accordance with an Ostwald ripening theory as they coarsened in time and eventually dissolved. The changes in defect density with time are depicted in Fig. 3 in which the density can be observed to decrease exponentially from $\sim 5 \times 10^{11}$ cm^{-2} to $\sim 3 \times 10^{9}$ cm^{-2} in a 4 h annealing interval. Conversely, in samples containing both B^+ and Ge^+ the extended defects were ephemeral and were not visible in the structure after annealing for 30 min. In Fig. 4, the defect evolution can be seen. The microstructure during the first 5 min of annealing appeared to be very similar to that of the experimental control in that tiny dot-like defects [9] existed in the structure. Nevertheless, 10 min into the annealing process distinct differences in the microstructures were apparent since the defects began to dissolve rather than evolve as those extended defects observed in samples containing Ge^+ only. In samples annealed for 30 min, virtually no defects were observed. Defect density as a function of time is depicted in Fig. 5. A spike anneal at 750 °C resulted in a defect density of 3.5×10^{11} cm^{-2} which decreased to 1.0×10^{11} cm^{-2} after 20 min of annealing. The density then plummeted to levels below the TEM detection limit. The considerable differences observed in the defect evolution for samples with and without boron in the lattice, strongly suggest the boron presence has an effect on the defect behavior [10]. Fig. 6 shows the boron concentration–depth profiles obtained from SIMS analyses. The boron pile up in the EOR region within in the first 10 min of annealing, at a depth of 27 nm, is indicative of boron gettering to the EOR [11]. After 30 min of annealing, the bump

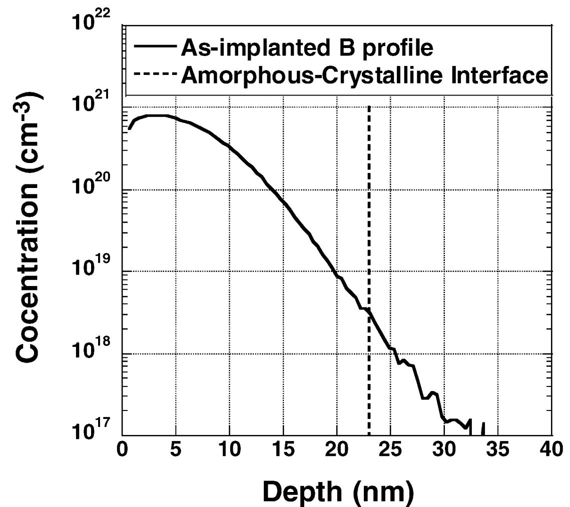

Fig. 1. As-implanted boron concentration–depth profile for the sample containing a 1 keV, 1×10^{15} cm^{-2} B^+ and 10 keV, 1×10^{15} cm^{-2} Ge^+ implants, indicating the amorphous–crystalline interface.

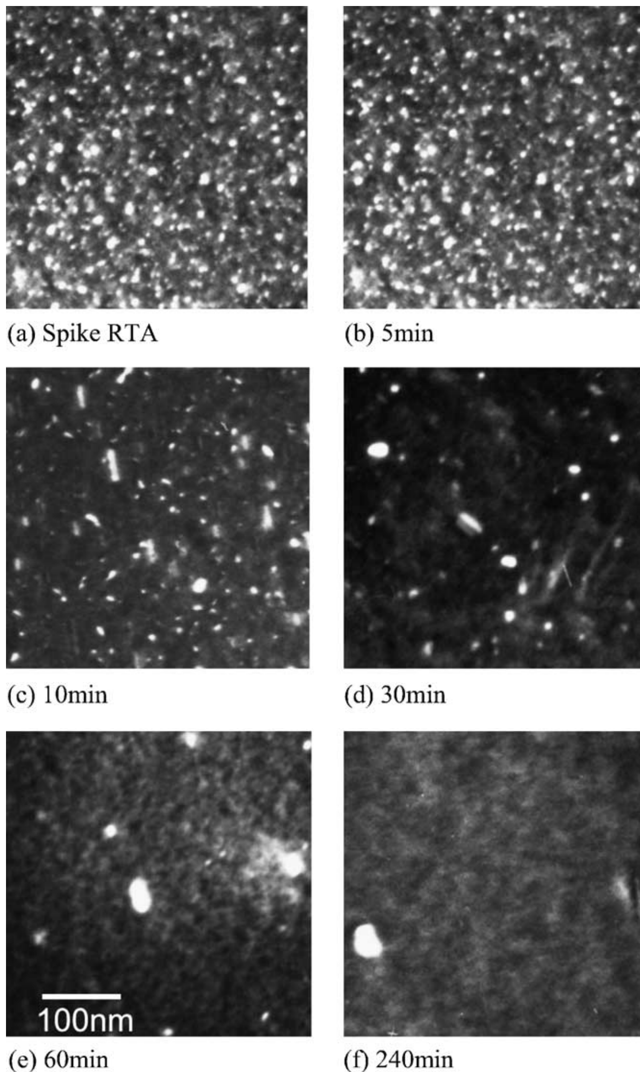

(a) Spike RTA (b) 5min (c) 10min (d) 30min (e) 60min (f) 240min

Fig. 2. PTEM WBDF images taken at g_{220} imaging conditions of the extended defects for samples containing 10 keV, $1 \times 10^{15}\,cm^{-2}$ Ge^+ implants. Annealed at 750 °C.

in the profile is gone. This concurs with the PTEM analysis that demonstrated dissolution of the EOR damage. Another prominent feature in the SIMS plots is the enhanced diffusion between 5 and 10 min which resulted in an approximate 15 nm increase in junction depth. Prior to and beyond this time, the observed diffusion is considerably less with a mere junction motion of approximately 5 nm during the 20 min interval between 10 and 30 min, suggestive of a transient diffusion enhancement. This observation is therefore indicative of a transitory supersaturation of silicon interstitials in the 5–10-min annealing interval. Further examination of the SIMS plots reveals that concentrations exceeding $5 \times 10^{18}\,cm^{-3}$ have moved in the direction of the Si/SiO_2 interface for all profiles, similar to reports by Duffy et al. [12]. Progressive motion toward the surface on the order of 1 and 1.9 nm were achieved for the spike and 30 min anneals, respectively. Additionally, there were increased boron concentrations at the surface to values on the order of $1 \times 10^{21}\,cm^{-3}$ for the 10

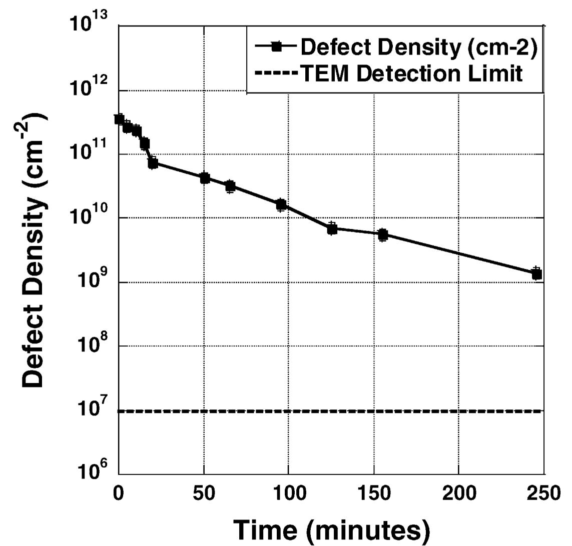

Fig. 3. Defect density as a function of annealing time for samples containing 10 keV, $1 \times 10^{15}\,cm^{-2}$ Ge^+ implants. Annealed at 750 °C.

and 30 min anneals. These characteristics are consistent with previous reports of boron uphill diffusion [12,13] and may be indicative of such a phenomenon. However, extraction of the boron dose from the SIMS profiles indicated lower retained boron doses than the implanted dose. The retained dose decreased with increasing anneal-times, suggesting boron dose loss may have occurred during annealing, which could also account for the motion of the profiles to the surface. Comparison of the increase in the boron surface levels between

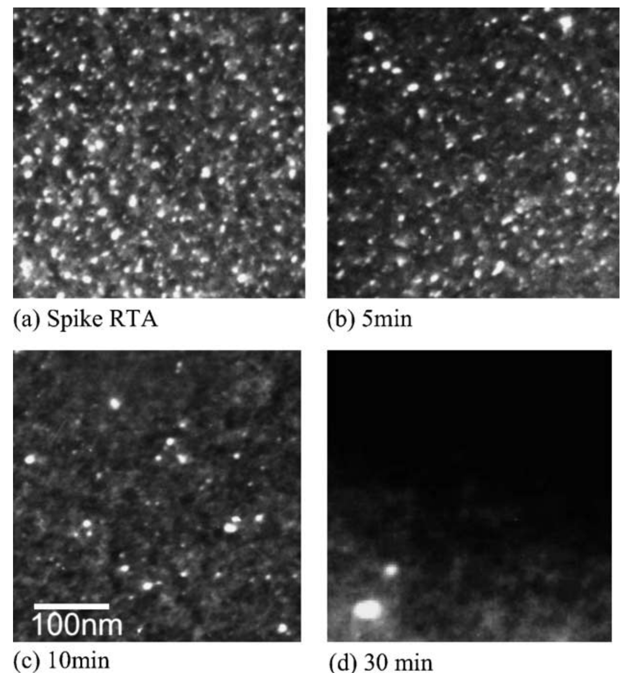

(a) Spike RTA (b) 5min (c) 10min (d) 30 min

Fig. 4. PTEM WBDF images taken at g_{220} imaging conditions of the extended defects for samples containing 1 keV, $1 \times 10^{15}\,cm^{-2}$ B^+ and 10 keV, $1 \times 10^{15}\,cm^{-2}$ Ge^+ implants. Annealed at 750 °C.

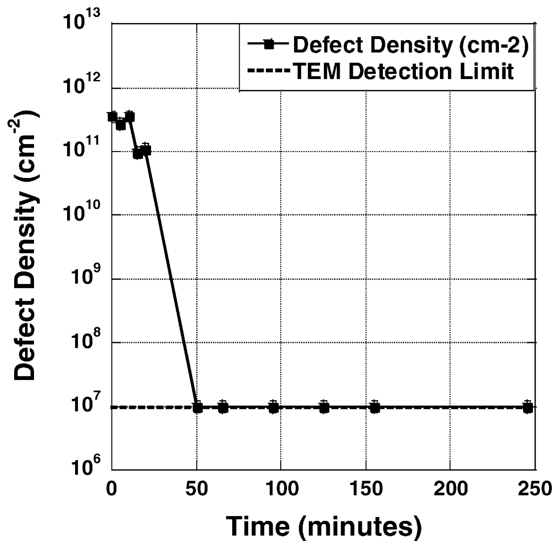

Fig. 5. Defect density as a function of annealing time for samples containing 1 keV, 1×10^{15} cm^{-2} B$^+$ and 10 keV, 1×10^{15} cm^{-2} Ge$^+$ implants. Annealed at 750 °C.

the 5–10-min and 10–30-min anneal time intervals, clearly indicates significantly more boron diffusion to the surface occurred between 5 and 10 min. In accordance with the theories put forth by Cowern et al. [14], in which they suggest that the interstitial supersaturation gradient provides efficient boron transport to the surface, a much higher interstitial flux to the surface must exist in the 5–10-min interval. This high flux is indicative of a steeper interstitial gradient from the defect layer to the surface. The smaller increase in boron surface concentration between 10 and 30 min therefore represents a decline in the surface interstitial flux and thus a reduction in the driving force for interstitial diffusion. These observations reveal that the interstitial supersaturation levels in the lattice falls with progressive annealing, supported by the reduced diffusion in the tail of the profile between 10 and 30 min, mentioned above. This time frame also coincides with the rapid release of interstitials from the EOR damage which is also indicative of a reduction in interstitial supersaturation. Extended defects require high levels of interstitial supersaturation in their vicinity in order to exist as stable structures. Should these supersaturation concentrations fall, defect dissolution occurs releasing the trapped interstitials, in an attempt to sustain the necessary interstitial levels. Consequently, defect evolution into more stable structures cannot occur. The experimental results herein demonstrate that for samples containing boron, rapid defect dissolution occurs, which is symptomatic of a drastic decrease in interstitial supersaturation. On the contrary, in samples without boron, the EOR damage was seen to undergo Ostwald ripening and evolved into stable dislocation loops, suggestive of an adequate interstitial supersaturation. Based on these recognized differences in behavior, it is reasonable to infer that the boron presence influences the interstitial supersaturation and hence the EOR defect evolution. It is postulated that this occurs by boron clustering with the interstitial atoms. The boron implant conditions employed in this experiment confines the boron atoms to the vicinity of the surface resulting in high surface levels of $\sim 1 \times 10^{21}$ cm^{-3}. Furthermore, high concentrations are also attained in the EOR region. It is well established that boron interstitial clustering occurs when a highly doped region is subjected to an interstitial supersaturation [6]. At 750 °C, the interstitial supersaturation is on the order of 1×10^4 according to the findings of Cowern et al. [15]. Therefore, the necessary conditions exist to enable clustering effects and boron interstitial cluster (BIC) formation. BICs grow by binding interstitials until a high supersaturation is sustained. [16,17] Recent experiments conducted by Mannino et al. [17] demonstrate that the interstitial supersaturation in samples containing boron is considerably lower when BICs are formed. It is therefore postulated that because the boron is in close enough proximity to the EOR, the BICs compete with the EOR defects for the interstitial supersaturation. [18,19] Hence, the supersaturation in the defect band falls to levels that are too low to support the extended defect existence and evolution, so they dissolve. BICs are known to have a detrimental effect on the electrical properties of the doped silicon host due to boron electrical deactivation [18,20] and carrier concentration mobility lowering. [21] Understanding the electrical behavior of the doped material is therefore essential to gaining further insight into the processes governing the defect evolution. Fig. 7 is the boron activation data represented as sheet resistance as a function of anneal-time. The most striking feature of the plot is the rapidity with which substitutional boron deactivates; demonstrated by the sharp increase in sheet resistance within the first 15 min of annealing. A spike anneal at 750 °C achieved a sheet resistance of $\sim$490Ω/□ which increased to $\sim$1750Ω/□ where it saturated. Measurements conducted on samples annealed for 4 h exhibited no improvements in boron activation, suggestive of the existence of boron in a very stable, inactive configuration. BICs have been shown to be very stable, existing up to 4 h after TED at 800 °C [6,21]. These deactivation characteristics

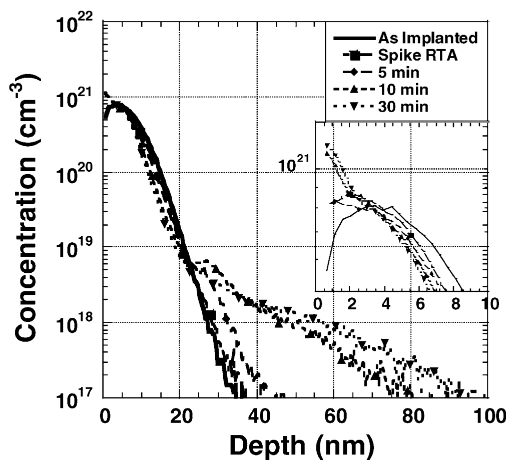

Fig. 6. Boron concentration–depth profiles for samples containing a 1 keV, 1×10^{15} cm^{-2} B$^+$ and 10 keV, 1×10^{15} cm^{-2} Ge$^+$ implants. Annealed at 750 °C.

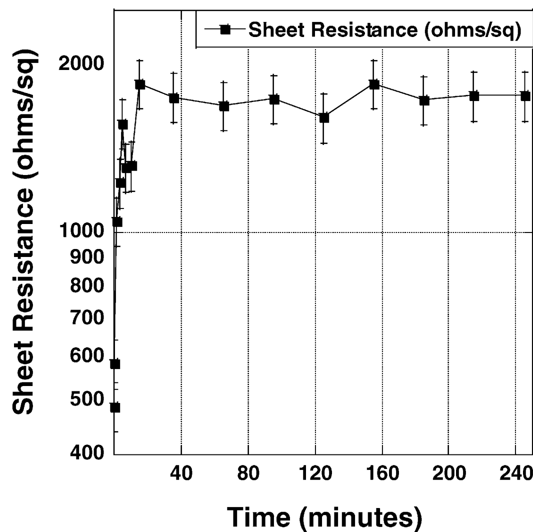

Fig. 7. Sheet Resistance vs. anneal time for samples containing a 1 keV, $1 \times 10^{15}\,cm^{-2}$ B^+ and 10 keV, $1 \times 10^{15}\,cm^{-2}$ Ge^+ implants. Annealed at 750 °C.

are consistent with the formation BICs and strongly suggest their occurrence. The fact that the deactivation process saturates implies that the interstitial saturation levels may have fallen to levels that are to low to support further BIC formation. This coincides with the fall in supersaturation observed in the SIMS data as well as the rapid dissolution of the EOR associated with reduced interstitial levels. Typically, BICs are immobile and stationary peak concentrations observed in SIMS profiles are characteristic of the existence of these clusters. The SIMS results obtained in these experiments however, do not exhibit this characteristic. A possible explanation for this is that the immobile regions are hidden. An estimate of the clustered concentrations can be extracted from the electrical data assuming that the inactive concentrations are clustered. A more accurate calculation is obtained by utilizing the total retained dose determined from the SIMS analysis. On this basis, the clustered concentrations were estimated at $1 \times 10^{20}\,cm^{-3}$, which is below the maximum boron concentrations achieved by the implant. Consequently, the immobile portions of the profiles are not visible. The clustered boron concentrations are also two orders of magnitude higher than the boron levels in the EOR, suggesting that the boron deactivation is not confined to the EOR region. Deactivation of the boron atoms in the regrown crystal therefore necessitates the migration of interstitial atoms from the EOR to regions of high boron concentrations [9]. However, the driving force for interstitial motion is not clear. One possibility is interstitial annihilation at the surface. It is evident in the experimental control that interstitial annihilation at the surface does not deplete the supersaturation in the EOR sufficiently for defect dissolution [22]. Hence, it is reasonable to assume that surface does not play a role in the reduced interstitial levels in samples containing boron and thus, in the interstitial migration from the EOR region. The tensile strains associated with the initially high substitutional boron concentrations may induce interstitial diffusion from the EOR to compensate for the strain. This migration is plausible since the EOR region is situated such that it is not isolated from the effects of the strained layer. The migrating interstitials subsequently interact with the boron in the highly doped, strained area to form BICs which continue to bind interstitials competing with the EOR defects for the interstitial supersaturation. The EOR defects therefore never evolve into more stable structures.

4. Conclusion

Boron presence in the vicinity of the EOR plays a fundamental role in the EOR defect evolution. The rapid dissolution process of the EOR damage in samples containing boron signifies a reduction in interstitial supersaturation which is attributed to the formation of boron interstitial clusters. It is postulated that the tensile strain associated with the initially high boron activation may induce interstitial migration from the EOR region to the strained layer, resulting in the BIC formation which results in a rapid deactivation process. Consequently, the supersaturation in the EOR falls to levels that are too low to sustain the extended defect evolution and the defects ultimately dissolve.

References

[1] A.E. Michel, W. Rausch, P.A. Ronsheim, R.K. Keitl, Appl. Phys. Lett. 50 (7) (1987) 417.
[2] L.H. Zhang, K.S. Jones, P.H. Chi, D.S. Simons, Appl. Phys. Lett. 67 (14) (19952025).
[3] H.G.A. Huizing, C.C.G. Visser, N.E.B. Cowern, P.A. Stolk, R.C.M. de Kruif, Appl. Phys. Lett. 69 (9) (1996) 1211.
[4] J.L. Benton, S. Libertino, P. Kringhoj, D.J. Eaglesham, J.M. Poate, J. Appl. Phys. 82 (1) (1997) 120.
[5] S. Coffa, S. Libertino, C. Spinella, Appl. Phys. Lett. 76 (3) (2000) 321.
[6] P.A. Stolk, H.-J. Gossmann, D.J. Eaglesham, D.C. Jacobson, J.M. Poate, H.S. Luftman, Appl. Phys. Lett. 66 (5), 570.
[7] S. Bharatan, J. Desrouches, K.S. Jones, Materials and Process Characterization of Ion Implantation, Ion Beam Press, 1997.
[8] S.H. Jain, P.B. Griffin, J.D. Plummer, J. Appl. Phys. 93 (2) (2003) 1060.
[9] B.J. Pawlak, R. Surdeanu, B. Colombeau, A.J. Smith, N.E.B. Cowern, R. Lindsay, W. Vandervorst, B. Brijs, O. Richard, F. Cristiano, Appl. Phys. Lett. 84 (12) (2004) 2055.
[10] T.E. Haynes, D.J. Eaglesham, P.A. Stolk, H-J. Gossmann, D.C. Jacobson, J.M. Poate, Appl. Phys. Lett. 69 (10) (1996) 1376.
[11] C. Bonafos, A. Claverie, D. Alquier, C. Bergaud, A. Martinez, L. Laanab, D. Mathiot, Appl. Phys. Lett. 71 (3) (1997) 365.
[12] R. Duffy, V.C. Venezia, H. Heringa, T.W.T. Husken, M.J.P. Hopstaken, N.E.B. Cowern, P.B. Griffin, C.C. Wang, Appl. Phys. Lett. 82 (21) (2003) 3647.
[13] H.C. Wang, C.C. Wang, C.S. Chang, T. Wang, P.B. Griffin, C. Diaz, IEEE Electr. Dev. Lett. 22 (2.) (2001).
[14] N.E.B. Cowern, B. Colombeau, R. Duffy, V. Venezia, C. Dachs, R. Lindsay, F. Cristiano, E. Lampin, A. Claverie, Mater. Res. Soc. Symp. Conf. Proc. 765 (2003) D.6.8.1.

[15] N.E.B. Cowern, G. Mannino, P.A. Stolk, F. Roozeboom, H.G.A. Huizing, J.G.M. van Berkum, F. Cristiano, A. Claverie, Phys. Rev. Lett. 82 (22) (1999) 4460.
[16] L. Pelaz, G.H. Gilmer, H-J. Gossmann, C.S. Rafferty, M. Jaraız, J. Barbolla, Appl. Phys. Lett. 74 (1999) 3657.
[17] G. Mannino, N.E.B. Cowern, F. Roozeboom, J.G.M. van Berkum, Appl. Phys. Lett. 76 (2000) 855.
[18] A.D. Lilak, S.K. Earles, M.E. Law, K.S. Jones, Appl. Phys. Lett. 74 (14) (1999) 2038.
[19] T.E. Haynes, D.J. Eaglesham, P.A. Stolk, H-J. Gossman, D.C. Jacobson, J.M. Poate, Appl. Phys. Lett. 69 (1996) 1376.
[20] N.E.B. Cowern, K.T.F. Janssen, H.F.F. Jos, J. Appl. Phys. 68 (12) (1990) 6191.
[21] S. Mirabella, E. Bruno, F. Priolo, D. De Salvador, E. Napolitani, A.V. Drigo, A. Carnera, Appl. Phys. Lett. 83 (4) (2003).
[22] A.C. King, A.F. Gutierrez, A.F. Saavedra, K.S. Jones, D. Downey, J. Appl. Phys. 93 (5) (2003) 2449.